Crystallization of 2H and 4H PbI$_2$ in Carbon Nanotubes of Varying Diameters and Morphologies

E. Flahaut,*,[†] J. Sloan,[‡,§,⊥] S. Friedrichs,[‡] A. I. Kirkland,[§] K. S. Coleman,[∥] V. C. Williams,[‡]
N. Hanson,[‡] J. L. Hutchison,[§] and M. L. H. Green[‡]

*Centre Interuniversitaire de Recherche d'Ingénierie sur les Matériaux, Université Paul Sabatier, UMR
CNRS 5085, Bât. 2Rl, 31062 Toulouse Cedex 9, France, Inorganic Chemistry Laboratory and Department
of Materials, University of Oxford, Parks Road, Oxford, OX1 3PH, United Kingdom, and Department of
Chemistry, University Science Laboratories, South Road, Durham, DH1 3LE, United Kingdom*

The crystallization of the complex halide PbI$_2$ in discrete and bundled single-walled carbon nanotubes (SWNTs), double-walled carbon nanotubes (DWNTs), and thicker walled nanotubes is described. The nanotubes were produced by either arc synthesis or catalytic chemical vapor deposition. The obtained crystals could be described in terms of 1D fragments derived principally from the 2H form of PbI$_2$, although some evidence for the formation of fragments derived from 4H PbI$_2$ in some nanotubes was observed. The crystallization inside nanotubes was compared to the crystallization behavior of bulk PbI$_2$ as determined by X-ray powder diffraction measurements obtained under comparable heating conditions. While the 2H to 4H polytype transition is clearly observable in bulk PbI$_2$, stacking behavior correlated with this type of polytypism was only very occasionally observed within nanotubes, suggesting that crystallizing PbI$_2$ within nanotubes has a tendency to order the halide into the 2H form. Additionally, PbI$_2$ apparently does not crystallize in rigid narrow DWNTs with internal diameters of less than 2 nm. Raman studies performed on the PbI$_2$-filled nanotubes show that the ratio of intensity of the D and G bands generally increases after filling and that both the RBM peaks and the G band are slightly upshifted.

Introduction

A wide variety of metal oxides, metal halides, and other materials may be introduced into opened multiwalled or single-walled carbon nanotubes (SWNTs) from the melt.[1,2] These experiments have permitted the study of the crystal growth of low-dimensional materials whereby the incorporated crystals are constrained to just a few atomic layers in cross-section by the internal van der Waals surface of the carbon nanotubes.[3] The ability of carbon nanotubes, in particular SWNTs, to allow crystal growth on such a scale is fostered by their extremely small diameters, and for nanotubes with internal diameters as small as 0.8−1.4 nm or less, encapsulation results in a profound change of the structural chemistry of the included material relative to its bulk form, resulting in either a systematic reduction of coordination without an overall change in structure, as in the case of 2 × 2 and 3 × 3 KI incorporated within 1.4 and 1.6 nm diameter SWNTs, respectively,[4,5] or a complete change in local structural chemistry, as observed for BaI$_2$ and CoI$_2$ formed within SWNTs.[6,7]

Changes in the local crystal chemistry of nanotube-incorporated crystals have been observed directly by high-resolution transmission electron microscopy (HRTEM) but have also been predicted from ab initio calculations. For one of the simpler binary halide structures, rock salt KI, Wilson established a phase diagram for crystal growth according to SWNT capillary diameter in the range 1.0−1.8 nm and also in terms of calculated minimum energy for 1D crystals.[8] The resulting 1D crystals were either of the form 2 × 2 or 3 × 3 atomic layers in cross-section or tube-like crystals consisting of repeating twisted three-, five-, or seven-membered rings or ordered six-membered rings extending along their capillaries.[8] A further factor that must be taken into account is the relative complexity of the crystal chemistry of the introduced materials which varies as a function of stoichiometry and anion−cation size ratio and as the bond strength changes. For example, we have shown that 3D network halides of the form LnCl$_3$ and ThCl$_4$ crystallize as reduced six-coordinate polyhedral chains[8,9] and also that the layered halide CoI$_2$ forms a doubled tetrahedral chain structure within SWNTs.[7] Associated with these local changes we anticipate

[†] Université Paul Sabatier.
[‡] Inorganic Chemistry Laboratory, University of Oxford.
[§] Department of Materials, University of Oxford.
[⊥] Now at Advanced Technology Institute, School of Electronics and Physical Sciences, University of Surrey, Guildford GU2 7NK, U.K.
[∥] Department of Chemistry, University Science Laboratories.

(1) Ajayan, P. M.; Iijima, S. *Nature* **1993**, *361*, 333.
(2) Sloan, J.; Wright, D. M.; Woo, H. G.; Bailey, S. R.; Brown, G.; York, A. P. E.; Coleman, K. S.; Hutchison, J. L.; Green, M. L. H. *Chem. Commun.* **1999**, 699.
(3) Sloan, J.; Kirkland, A. I.; Hutchison, J. L.; Green, M. L. H. *Chem. Commun.* **2002**, 1319.
(4) Sloan, J.; Novotny, M.; Bailey, S. R.; Brown, G.; Xu, C.; Williams, V. C.; Friedrichs, S.; Flahaut, E.; Callendar, R. L.; York, A. P. E.; Coleman, K. S.; Green, M. L. H. *Chem. Phys. Lett.* **2000**, *329*, 61.
(5) Meyer, R. R.; Sloan, J.; Dunin-Borkowski, R. E.; Novotny, M. C.; Bailey, S. R.; Hutchison, J. L.; Green, M. L. H. *Science* **2000**, *289*, 1324.
(6) Sloan, J.; Grosvenor, S. J.; Friedrichs, S.; Kirkland, A. I.; Hutchison, J. L.; Green, M. L. H. *Angew. Chem., Int. Ed.* **2002**, *41*, 1156.
(7) Philp, E.; Sloan, J.; Kirkland, A. I.; Meyer, R. R.; Friedrichs, S.; Hutchison, J. L.; Green, M. L. H. *Nat. Mater.* **2003**, *2*, 788.
(8) Wilson, M. *Chem. Phys. Lett.* **2002**, *366*, 504.

a concomitant change in the resulting physical properties of the included materials, although the first published density functional theory calculation on 2×2 KI intercalated within a (10,10) SWNT has concentrated on the charge-transfer phenomena occurring between KI and the nanotube rather than on the intrinsic electronic properties of the included nanocrystal.[10]

In the present study, we describe the crystallization behavior of the complex layered halide PbI_2 in SWNTs and double-walled carbon nanotubes (DWNTs) of differing diameters. Nominally, PbI_2 conforms to the layered CdI_2 structural archetype, although it exhibits extensive twinning and polytypism. Ordered polytypes of PbI_2, of which the 2H, 4H, and 12R forms are the most common (Figure 1a–c), can be produced as a function of its thermal treatment.[11] Bulk PbI_2 is a direct band gap semiconductor with an energy gap in the range $2.2-2.6$ eV with potential application as a room-temperature detector material for both γ- and X-radiation.[12] The ability of crystalline PbI_2 to detect γ- and X-radiation efficiently is strongly correlated with the type and local concentration of polytype defects.[13,14] Additionally, as the detector leakage current is proportional to the conductivity of the material and good detectors are expected to have a low leakage current value, the electrical conductivity of the material should be as high as possible. Reducing the extent of polytype formation on a local scale may thus be a way to improve the performances of such materials. On a more confined scale, colloids or nanoparticles of PbI_2 show a variation in the size-related excitonic absorption in the $480-490$ nm range which has also been partly attributed to polytype formation.[15,16] This effect should be reduced as the cross section of the PbI_2 particles is reduced as the extent of polytypism is limited in effect by the particle size. We therefore give special attention in this paper to the degree of PbI_2 polytype formation formed within SWNTs and DWNTs as a function of the diameter of the encapsulating nanotube.

SWNTs produced by catalytic chemical vapor deposition (CCVD)[17] are known to have a wider diameter distribution than SWNTs prepared by arc discharge[18] or laser ablation.[19] Additionally, double-walled carbon nanotubes produced by various catalytic routes also vary considerably in diameter,

and this should have a significant effect on the obtained crystal growth. Recently, for example, we have shown that alkali halides have distorted or defect crystal growth behavior in wider DWNTs.[20] The PbI_2 fillings were characterized by a combination of conventional HRTEM, improved resolution through-focal series HRTEM image restoration, which we previously used in the characterization of SWNT encapsulated 3×3 KI[5] and the 1D CoI_2[7] nanocrystals, among others, and Raman spectroscopy studies. We also briefly describe the washing-out properties of the PbI_2-filled nanotubes resulting in opened, unfilled SWNTs and DWNTs.

Experimental Section

The bulk crystallization behavior of the PbI_2 material (99.999% purity, Aldrich) used to fill the SWNT and DWNT samples from room temperature to a maximum temperature of 620 K was determined by dynamic X-ray powder diffraction (XRD) under He at a ramping rate of 0.1 K min^{-1}. XRD powder patterns were obtained at temperature intervals of 10 K between 400 and 460 K and then at intervals of ca. 50 K from 520 to 620 K during the ramping stage. Each XRD pattern was obtained over a dwell period of 1 h at each measurement stage. Symmetrical cooling rates and XRD measurements were obtained using approximately similar cooling rates. XRD analysis was performed using a Bruker D5005 diffractometer with Cu Kα radiation, fitted with a Göbel mirror and an Anton Paar HTK 1200 furnace.

SWNTs were prepared by arc synthesis using a Ni:Y-doped anode using a modified Krätschmer–Huffman arc synthesis procedure.[21] DWNTs were prepared using two different catalysts: (i) a $Mg_{0.9}Co_{0.1}O$ solid solution known to yield a mixture of SWNTs and DWNTs[17] or (ii) a $Mg_{0.99}Co_{0.0075}Mo_{0.0025}O$ catalyst yielding around 80% DWNTs.[22] Both catalysts were reduced at 1000 °C in a mixture of H_2 and CH_4 containing 18 mol % of CH_4. The resulting composite powder was then soaked in a concentrated aqueous HCl solution to separate the nanotubes by dissolving all the remaining oxide material as well as unprotected metal particles.[20] The acidic suspensions were filtered and washed with deionized water until neutrality. The samples were dried overnight at 80 °C in air. SWNT and DWNT samples were filled using a high filling yield capillary wetting technique.[1,2,24] SWNTs or DWNTs were mixed and gently ground together with PbI_2. The mixture was vacuum-sealed in a quartz ampule, which was heated in a programmed furnace at 5 K min^{-1} to 723 K (i.e., above the melting point of PbI_2), followed by a dwell at this temperature for 5 h, followed by cooling to 643 K at 0.1 K min^{-1} and then down to room temperature at 1 K min^{-1}. Extraneous PbI_2 was removed by sonicating the filled nanotubes in a concentrated NaOH solution (6 M) for 30 s, immediately followed by filtration on a polycarbonate membrane. In the case of the complete removal of PbI_2 from both outside and inside the SWNTs and DWNTs, the filled specimens were refluxed overnight at 90 °C in a round-bottom flask containing 10 M NaOH. The emptied nanotubes were then washed on a polycarbonate membrane

   (9) Xu, C.; Sloan, J.; Brown, G.; Bailey, S. R.; Williams, V. C.; Friedrichs, S.; Coleman, K. S.; Flahaut, E.; Hutchison, J. L.; Dunin-Borkowski, R. E.; Green, M. L. H. *Chem. Commun.* **2000**, 2427.
  (10) Yam, C. Y.; Ma, C. C.; Wang, X. J.; Chen, G. H. *Appl. Phys. Lett.* **2004**, *85*, 4484.
  (11) Konings, R. J. M.; Cordefunke, E. H. P.; van der Laan, R. R. *J. Alloys Compd.* **1995**, *230*, 85.
  (12) Vessid, N.; An, C. Y.; Ferreria da Silva, A.; Pinto de Souza, J. I. *Mater. Res.* **1999**, *2*, 279.
  (13) Deich, M.; Roth, M. *Nucl. Instrum. Methods Phys. Res.* **1996**, *380*, 169.
  (14) Fornaro, L.; Saucedo, E.; Mussio, L.; Gancharov, A.; Guimaraes, F.; Hernandes, A. *IEEE Trans. Nucl. Sci.* **2002**, *49*, 3300.
  (15) Saito, S.; Goto, T. *Phys. Rev. B* **1995**, *103*, 3218.
  (16) Sengupta, A.; Jiang, B.; Mandal, K. C.; Zhang, J. Z. *J. Phys. Chem. B* **1999**, *103*, 3128.
  (17) Flahaut, E.; Peigney, A.; Laurent, C.; Rousset, A. *J. Mater. Chem.* **2000**, *10*, 249.
  (18) Ajayan, P. M.; Lambert, J. M.; Bernier, P.; Barbedette, L.; Colliex, C.; Planeix, J. M. *Chem. Phys. Lett.* **1993**, *215*, 509.
  (19) Guo, T.; Nikolaev, P.; Thess, A.; Colbert, D. T.; Smalley, R. E. *Chem. Phys. Lett.* **1995**, *243*, 49.

  (20) Costa, P. M. F. J.; Friedrichs, S.; Sloan, J.; Green, M. L. H. *Chem. Mater.* **2005**, *17*, 3122.
  (21) Journet, C.; Maser, W. K.; Bernier, P.; Loiseau, A.; Lamy de la Chapelle, M.; Lefrant, S.; Derniard, P.; Fisher, J. E. *Nature* **1997**, *388*, 756.
  (22) Flahaut, E.; Bacsa, R.; Peigney, A.; Laurent, C. *Chem. Commun.* **2003**, 1442.
  (23) Flahaut, E.; Agnoli, F.; Sloan, J.; O'Connor, C.; Green, M. L. H. *Chem. Mater.* **2002**, *14*, 2553.
  (24) Brown, G.; Bailey, S. R.; Novotny, M.; Carter, R.; Flahaut, E.; Coleman, K. S.; Hutchison, J. L.; Green, M. L. H.; Sloan, J. *J. Appl. Phys. A* **2003**, *76*, 1.
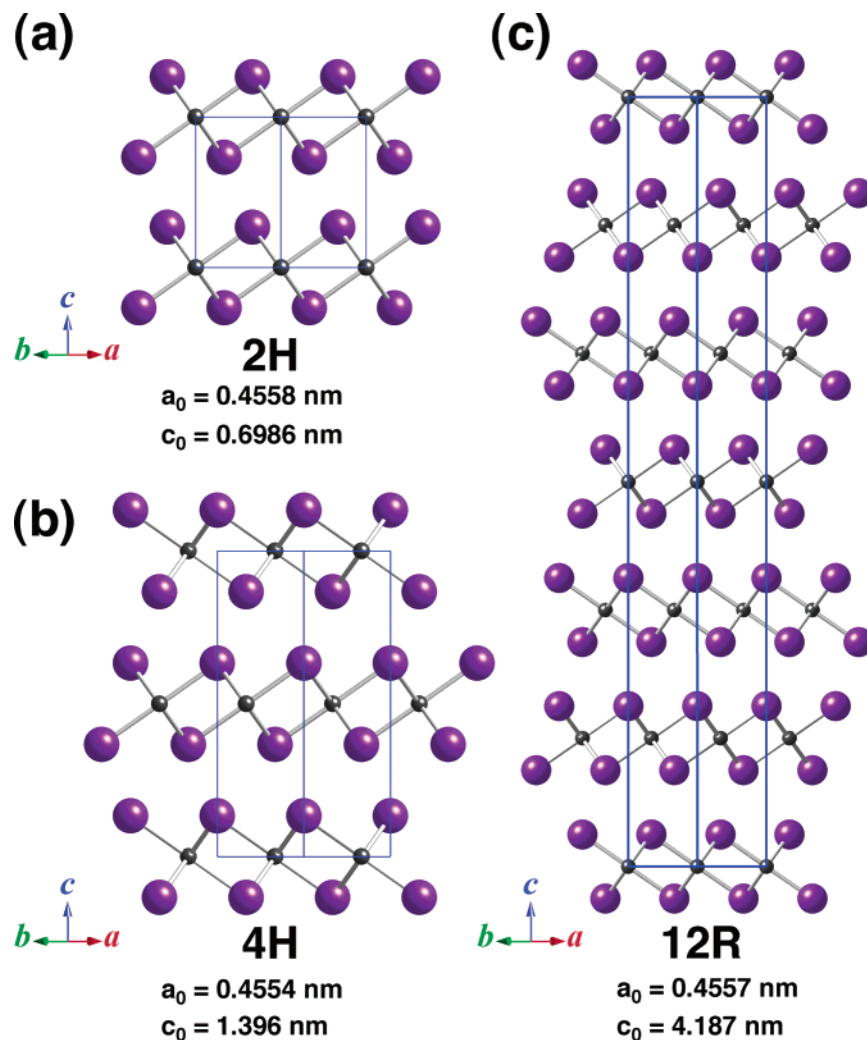
Figure 1. Idealized structural representations and lattice parameters of the three most stable polytypes of PbI_2: (a) 2H form, (b) 4H form, (c) 12R form. In this figure, iodine is depicted by purple spheres and lead is depicted by black spheres.

first with 10 M NaOH, then with 1 M NaOH, and finally with deionized water.

The filled samples were examined at 300 kV in a JEOL JEM-3000F HRTEM, which has a low spherical aberration coefficient C_s of 0.6 mm and a point resolution of 0.16 nm. Images were acquired digitally on a Gatan model 794 (1k × 1k) CCD camera, and the magnification was calibrated accurately using Si $\langle 110 \rangle$ lattice fringes. For selected samples, HRTEM focal series were produced and restorations of the phase of the complex exit plane wave function were obtained as previously described.[5,7,25,26] This technique has the advantage of producing restored HRTEM phase images at the information limit of the HRTEM (ca. 0.1 nm for our instrument) as opposed to the normal Scherzer limit (ca. 0.16 nm for the same instrument). Each phase image was produced from focal series of 20 images at 0.15 nm increments produced at ×600 000 with a final image being recorded for drift calibration and an exposure time of 0.5 s per image. Image simulations were performed using a standard multislice algorithm utilizing typical performance parameters for the 3000F HRTEM. Power spectra were computed directly from HRTEM lattice images using the proprietary Gatan Digital Micrograph software. Electron diffraction patterns were calculated using either the Single-Crystal diffraction program

available from CrystalMaker Software Ltd. or the program SimulaTEM. Energy-dispersive X-ray microanalysis (EDX) was performed with a LINK 'ISIS' system equipped with an Oxford Instruments Pentafet detector using a 0.5 nm diameter electron probe on both filled and washed nanotubes.

Raman spectra were recorded from filled nanotube samples at room temperature with a resolution of 2 cm^{-1} using either a Yvon Jobin Labram spectrometer, equipped with a 514.5 nm Ar$^+$ laser, or a micro-Raman spectrometer (Dilor) with backscattering geometry equipped with a 488 nm Ar$^+$ laser; both ran in a backscattered confocal arrangement. The abscissa was calibrated with a silicon standard.

Results

(i) X-ray Powder Diffraction Studies. The temperature-programmed X-ray diffraction experiment performed on bulk PbI₂ showed that the 2H to 4H transition is observed as expected at 440 ± 20 K[11] and therefore occurs over the heating conditions employed to fill the nanotubes (Figure 2). An initial XRD pattern obtained at room temperature (Figure 2a) shows that the as-supplied bulk PbI₂ has the $P\bar{3}m1$ 2H form,[27] and we observe that the partial transforma-

(25) Coene, W.; Janssen, G.; de Beeck, M. O.; Dyck, D. V. *Phys. Rev. Lett.* **1992**, *69*, 3743.

(26) Meyer, R. R.; Kirkland, A.; Saxton, O. *Ultramicroscopy* **2002**, *92*, 89.

(27) Palosz, B.; Steurer, W.; Schulz, H. *J. Phys.: Condens. Matter* **1990**, *2*, 5285.
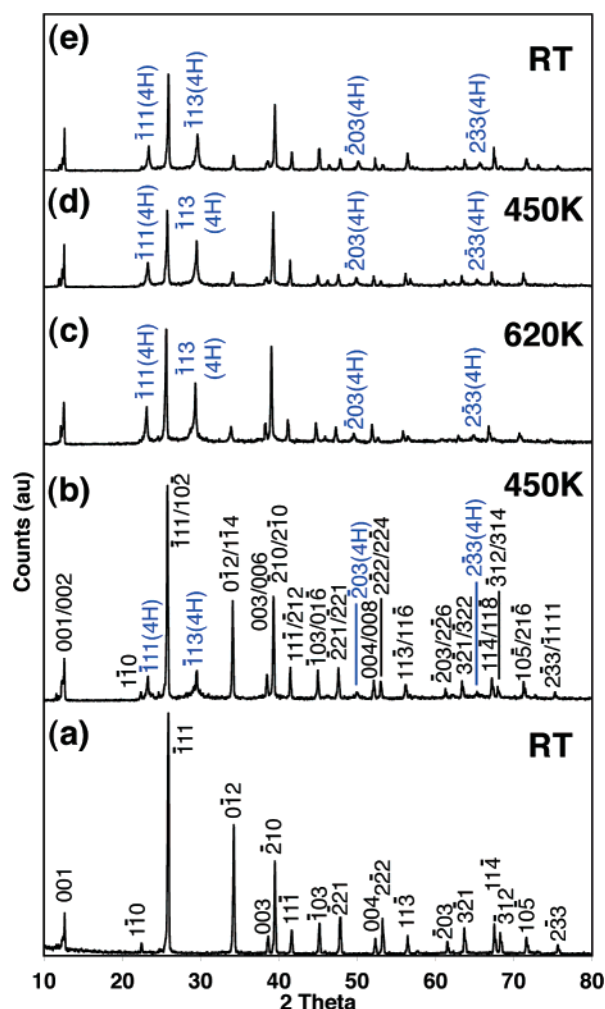
Figure 2. X-ray powder diffraction patterns obtained from temperature-programmed thermal treatment of PbI₂ used to fill SWNTs and DWNTs. (a) Starting pattern obtained at room temperature (RT) of as-supplied PbI₂ material consisting of 100% 2H−PbI₂. (b) XRD pattern obtained at 450 K. 4H lines are indicated in blue. Other lines are shown with combined 2H/4H indexing. (c−e) XRD patterns obtained at a maximum temperature of 620 K, during the cooling phase at 450 K, and final pattern obtained at RT following thermal treatment (4H lines only are indicated).

tion of this material to the $P6_3mc$ 4H form[27] starts to occur at 450 K as is indicated by the appearance of the unique $\bar{1}11$, $\bar{1}13$, $\bar{2}03$, and $2\bar{3}3$ 4H reflections in the powder patterns (Figure 2b). All of the remaining reflections correspond to a mixture of 2H and 4H polytypes as indexed in Figure 2b. As the temperature was raised from 450 to 620 K, the proportion of 4H increased to a maximum of ca. 70% of the overall mixture (Figure 2c). During the cooling stage (Figure 2d and e), a slight depletion of 4H PbI₂ was observed, but this did not decrease below 50% of the final product. This is consistent with a report stating that the transition of 4H back to 2H during cooling is slow.[11] No significant quantity of 12R (Figure 1c) was observed in any of the XRD powder patterns. Because of this observation and also the fact that the *c* lattice repeat of the $R\bar{3}m$ 12R PbI₂ form (i.e., 4.19 nm[28]) is large compared with the internal diameters of both SWNTs and DWNTs (typically 1−3 nm[21,22]), this polytype was not considered further.

   (ii) HRTEM of PbI₂ in Filled SWNTs and DWNTs. HRTEM shows that SWNTs fill continuously in very good

(28) Minagawa, T. *Acta Crystallogr. B* **1975**, *31*, 1222.

yield (ca. 60+%) with PbI₂ with DWNTs filling in somewhat lesser yield (ca. 50%). The encapsulated 1D PbI₂ crystals show strong (though not exclusive) preferred orientation with strongly scattering iodine {201} planes relative to the bulk 2H structure, aligning at an angle of ca. 60° to the SWNT axes and separated by 0.36 nm. In the example in Figure 3a {201} iodine planes can clearly be seen in the peripheral nanotubes in a SWNT bundle in which all the observed tubules are filled with PbI₂. In the detail in Figure 3b alternating {201} planes can be seen in adjacent SWNTs in the filled bundle, and these give rise to a pseudo-twinning effect in the corresponding power spectrum (i.e., Figure 3c) with the {201} planes being 'mirrored' (and indexed as 201′ etc., in Figure 3c) in adjacent SWNTs.

   The structural origin of SWNT encapsulated PbI₂ fragments can be determined more readily from different projections of discrete filled SWNTs, as shown in Figure 4a−i. As with the filled SWNT bundle, the {201} iodine layers are arranged at ca. 60° to the SWNT axis as shown in the detail (Figure 4b) and simulation (Figure 4c). This simulation was produced from the structure model derived in Figure 4d and e. The PbI₂ fragment was initially extracted as a three octahedra thick single slab of 2H PbI₂ (indicated in red, Figure 4g) from a discrete layer of 'infinite' PbI₂. Excess iodine ions are removed from the terminal chains of PbI₆ octahedra in order to produce a fragment consisting of a single chain of PbI₆ octahedra bounded by two chains of PbI₅ square pyramids, as indicated in the composite model in Figure 4e. This systematic reduction of coordination at the terminal polyhedra is essential in order to maintain charge balance (cf. TbCl₃[3,9] and BaI₂[6] in SWNTs). The iodine atom columns image with twice the comparative image contrast than the lead atom columns due to there being twice as many iodine atoms as lead atoms in projection, as shown in the end-on view or the resulting structure (Figure 4f), despite the higher atomic number of the latter (i.e., $Z = 53$ for I; $Z = 82$ for Pb). The resulting PbI₂ fragment is expected to be highly asymmetric in cross-section, and we anticipate that there will be a corresponding distortion in the cross-section of the encapsulating nanotube as shown in the end-on view (Figure 4f). This is similar to nanotube distortions that were reported for encapsulated 1D crystals of CoI₂ which reduces to a double tetrahedral chain of Co₂I₄ units with a diamond-like cross-section when encapsulated within SWNTs.[7] We can further confirm the microstructure of the 1D PbI₂ crystals from restored images of 1D crystals viewed in projections of discrete fragments viewed orthogonally to the projections reproduced in Figure 4a−e. In the top half of Figure 4g a reconstructed phase image obtained from a ca. 1.6 nm diameter SWNT filled with PbI₂ is reproduced. The relative orientation of this crystal is ca. 90° with respect to the orientation of the crystals depicted in Figure 4a and h (in Figure 3f, arrow **I** indicates the projection observed in Figure 4b while arrow **II** indicates the projection observed in Figure 4g). In this projection the encapsulated crystal fragment images as an alternating sequence of 1I−IPbI−1I and PbI−IPb layers in a structural arrangement similar to that reported for 1D BaI₂ crystals imaged within SWNTs.[6] A matching multislice HRTEM image simulation (i.e., Figure 4h) pro-
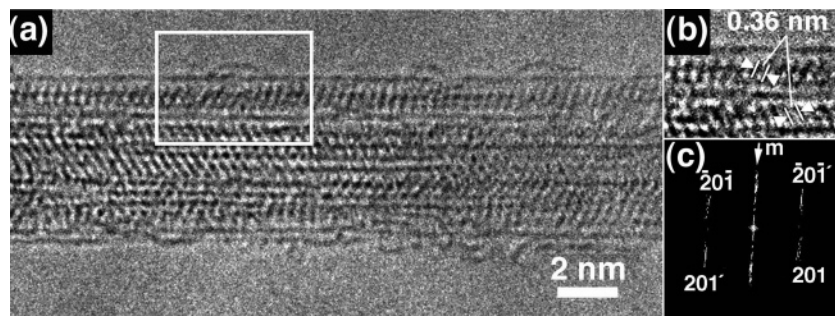
Figure 3. (a and b) conventional HRTEM image and detail (from boxed region) showing a bundle of SWNTs completely filled with PbI$_2$. (c) Power spectrum obtained from the same region as b). Pseudo-mirror plane (**m**) and coincident scattering from bundle are indicated by the small arrow.
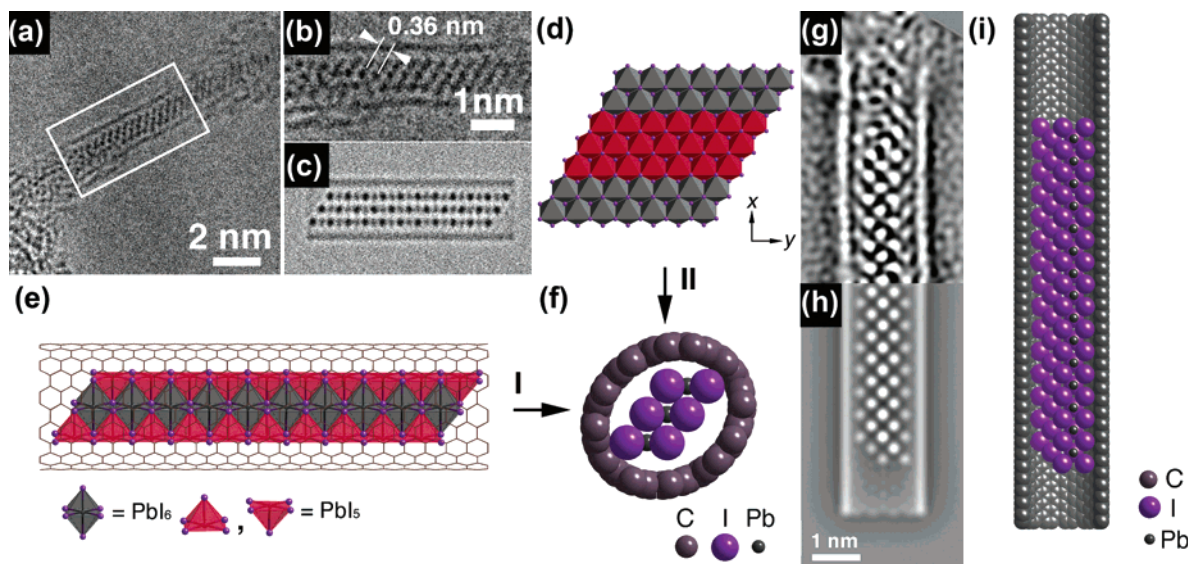

Figure 4. (a and b) conventional HRTEM image and detail (from boxed region) showing a PbI$_2$ 1D crystal formed within a 1.6 nm diameter SWNT. (c) Scherzer focus HRTEM image simulation based on the structure model in e. (d) Single layer of PbI$_2$ showing the 'origin' of the 1D fragment, indicated in red. (e) Composite model and (f) space-filling end-on view showing PbI$_2$ fragment inside a (12,12) SWNT. The latter shows how this tubule could distort in order to accommodate the derived asymmetric PbI$_2$ crystal fragment. The arrow **I** indicates the PbI$_2$ fragment projection in parts a–e. (g) Reconstructed phase image of a PbI$_2$ fragment formed in a 1.6 nm diameter SWNT. (h) Matching multislice simulation. (i) Composite model used to calculate the simulation in h. The projection of this fragment is indicated by arrow **II** in f.

duced from an equivalent fragment and a (12,12) SWNT (i.e., Figure 4i) shows good agreement between the experimental image and the proposed model. These types of crystal fragments should be regarded as corresponding to sub-2H-type structures (cf. Figure 1a) as, in cross section, the SWNT cannot accommodate more than a fragment of a single PbI$_2$ layer. Thus, neither 4H nor other PbI$_2$ polytypes can be accommodated in such narrow diameter SWNTs.

Microstructural behavior corresponding to 4H-type stacking was only occasionally observed to occur within slightly wider than average SWNTs, as shown in the example in Figure 5. Two lattice images, one obtained at close to Gaussian defocus (Figure 5a) and the second close to Scherzer defocus (Figure 5b), show alternating stacking behavior inside a short section of a SWNT tip. The cylindrical part of the SWNT is 2 nm in diameter, and in the second image (and in the enlargement in Figure 5c), two sets of twinned 0.32 nm fringes can be seen arranged at ca. 60° to the tubules axis in a herringbone arrangement. An image simulation, corresponding to a short section of a 4H fragment projected along ⟨110⟩ with respect to the bulk structure (cf. Figure 1b) and sliced orthogonal to this direction and embedded in a (15,15) SWNT, as shown in Figure 5d, is shown in Figure 5e. Side-on and end-on space-

filling models of the composite model are shown in Figure 5f and g, respectively. This crystal fragment corresponds to the thickness of a single unit cell of 4H PbI$_2$ projected along *c* and displaced by half a lattice parameter along the same direction. This was the only instance of 4H-type stacking that we were able to observe directly in either the filled SWNT or the CCVD DWNT samples.

PbI$_2$ did not appear to crystallize effectively in narrow DWNTs with internal diameters less than 2 nm. In the two examples shown in Figure 6a and b, noncrystallizing PbI$_2$ filling is observed in DWNTs with inner tubules of diameter ca. 1.2 nm in both cases. We previously only observed non- or partially crystallizing filling first in opened MWNTs[29] and, more recently, in SWNTs[2,30] when both were filled from the melt using binary eutectic mixtures of either KCl and UCl$_4$ (MWNTs and SWNTs) or AgCl and AgI (SWNTs only). In both instances one would anticipate noncrystallizing filling as a consequence of normal crystallization behavior of eutectic mixtures. The reason for the failure of binary PbI$_2$ to crystallize in narrow DWNTs is unclear but may be

(29) Sloan, J.; Cook, J.; Chu, A.; Zwiefka-Sibley, M.; Green, M. L. H.; Hutchison, J. L. *J. Solid State Chem.* **1998**, *140*, 83.
(30) Sloan, J.; Kirkland, A. I.; Hutchison, J. L.; Green, M. L. H. *C. R. Phys.* **2003**, *4*, 1063.
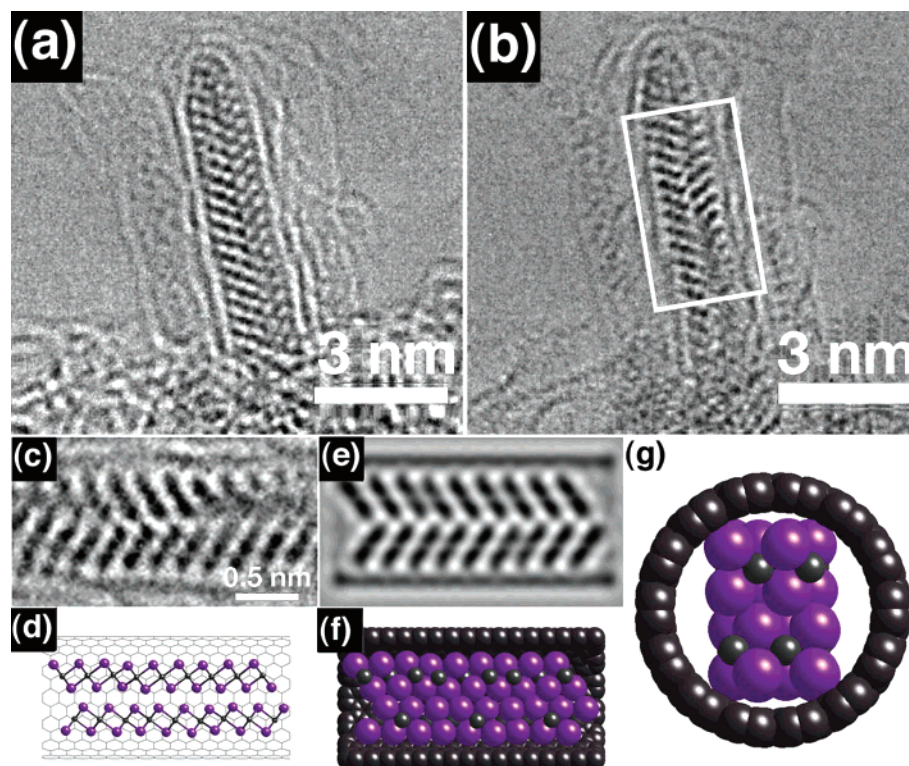
Figure 5. (a and b) Gaussian and Scherzer defocus images of a tip of a SWNT containing PbI_2. (c) Detail from boxed region in b showing the herringbone arrangement of the encapsulate microstructure. (d) Suggested structural arrangement of the 'nanotwin' consisting of a small fragment of 4H PbI_2 (cf. Figure 1b). (e) Scherzer defocus simulation obtained from the structure model in (d). (f and g) Cutaway and end-on space-filling representations on the nanotwin composite.
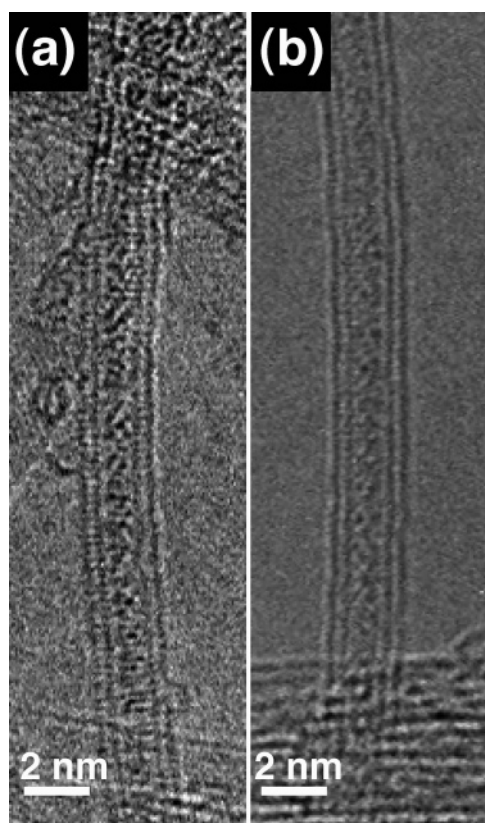

Figure 6. (a and b) Two examples of HRTEM images obtained near to Scherzer defocus of narrow DWNTs filled with noncrystallizing PbI_2.

associated with the greater structural rigidity of these tubules compared to SWNTs.[31] The two PbI_2 fragments imaged in Figure 4 are asymmetric when viewed in a projection along the SWNT cavity (i.e., Figure 4f), and we expect that this will cause an elliptical distortion of the encapsulating nanotube as similarly reported for CoI_2.[7] The failure of PbI_2 to crystallize in narrow DWNTs may be associated with the inability of the hot tubules to distort in order to accommodate asymmetric crystal fragments of the form represented in Figure 4, resulting instead in the noncrystallizing filling observed in Figure 6a and b.

In larger diameter DWNTs PbI_2 filling showed a much greater tendency to crystallize and virtually all fillings observed in nanotubes with a diameter greater than ca. 2 nm were crystalline. In the example in Figure 7a an ordered PbI_2 fragment can be seen encapsulated within a DWNT consisting of a ca. 1.8 nm diameter inner tubule and a ca. 2.5 nm diameter outer tubule. A power spectrum (Figure 7b) obtained from the indicated region in Figure 6a indicates that this fragment is imaged parallel to a $\langle 121 \rangle$ relative projection with respect to bulk 2H PbI_2 and is a similar orientation and fragment to that described in Figures 3j and k. The microstructure of this fragment is less distinct, although $\{\bar{1}01\}$ lattice planes can be seen to be oriented at an angle of ca. 45° to the DWNT axis, consistent with this orientation. The lack of clarity in the microstructure is possibly due to the crystal being slightly rotated about the axis of the DWNT relative to the crystal shown in Figure 4h. The assembled model in Figure 7d, consisting of the indicated PbI_2 fragment and a (13,13)SWNT@(19,19)SWNT DWNT pair, produces a calculated power spectrum that is in good agreement with the experimental power spectrum

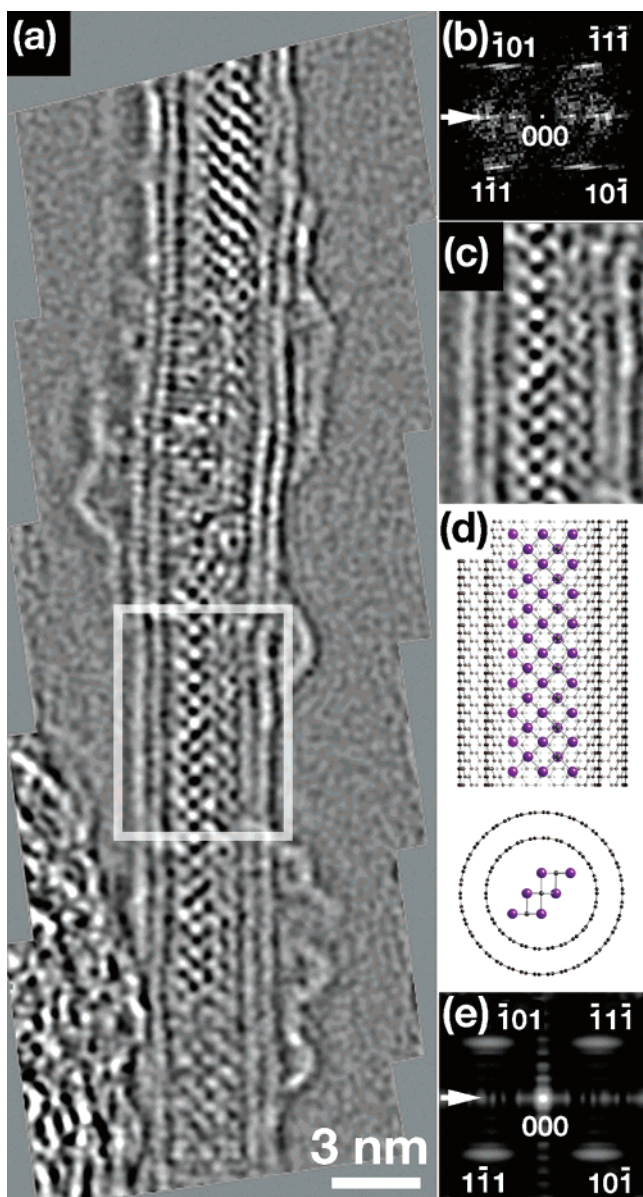(31) Shen, L.; Li, J. *Phys. Rev. B* **2005**, *71*, 025412-1.

Figure 7. (a) Phase image of a 1.7 nm i.d. DWNT continuously filled with crystalline PbI$_2$. (b) Experimental power spectrum obtained from the indicated region in a. (c) Detail of the indicated region in a. (d) Structure model derived from c. (e) Power spectrum calculated from the model in d.

in Figure 7b.

In Figure 8a we see a conventional HRTEM image of a wider DWNT in which the inner tube is ca. 2.5 nm in diameter and the outer tube is ca. 3.2 nm in diameter. The enlarged detail in Figure 8b and filtered image in Figure 8c both indicate that the filling is highly crystalline. The inset power spectrum in Figure 8a reveals that the encapsulated crystal is projected parallel to $\langle 121 \rangle$ with respect to the bulk form of 2H PbI$_2$ with the strong $\bar{2}10$ reflections aligning parallel to the DWNT axis. In this instance the inner DWNT is wide enough to accommodate fragments of three octahedral layers of PbI$_2$ as indicated in the composite model displayed in cutaway and end-on projections in Figure 8d and e, respectively. The power spectrum (inset, Figure 8a) and microstructure (Figure 8b and c) indicate that the layer stacking corresponds to the 2H form (cf. Figures 1a and 7e) and not the 4H form. Good agreement is obtained between an image simulation (i.e., Figure 8f) produced for ap-

proximately similar defocus with the experimental image (i.e., Figure 8c) from the composite PbI$_2$-DWNT model reproduced in Figure 8d and e. The DWNT in Figure 8d and e was modeled from a (19,19)SWNT@(24,24)SWNT pair. A further interesting point about the encapsulating nanotube is that on one wall there is an additional carbon layer, as indicated by the yellow arrow in Figure 8c. This may be due to the DWNT taking on a scroll-like structure rather than the more typical Russian Doll-type DWNT structure as indicated in Figure 8e, although this would be the first observation of this structure in a CNT with such a low number of walls. This effect could also be due to the presence of an incomplete partial layer of graphene formed on one side of the DWNT only.

In Figure 9a and b a restored phase image and detail of DWNT consisting of a 2.5 nm diameter inner tubule and a 3.2 nm diameter outer tubule filled with crystalline PbI$_2$ are shown, respectively. This is a similar-sized filled DWNT to the example shown in Figure 8, although the projection of the encapsulated crystal differs from the crystal fragment projection in Figure 8 as it is now viewed parallel to $\langle \bar{1}2\bar{1} \rangle$. This direction is not equivalent to $\langle 121 \rangle$ due to the low symmetry of the 2H PbI$_2$ structure. The power spectrum (Figure 9c), obtained from the indicated region in Figure 9a, reveals that, in common with the crystal fragment in Figure 8, the $\bar{2}10$ reflections align parallel to the DWNT axis. The corresponding microstructure in Figure 8b however differs considerably from the microstructure in Figure 9b due to the former being rotated clockwise about the axis of the DWNT by ca. 90° with respect to the latter, resulting in the fragment (similarly modeled in a (19,19)SWNT@(24,-24)SWNT pair) in Figure 8d and e. A multislice simulation (Figure 9f) produced from this model provides a fair agreement with the experimental image in Figure 9b, although alternating layers of atoms in the experimental image are blurred. This is possibly due to the fragment being tilted relative to an ideal $\langle \bar{1}2\bar{1} \rangle$ projection. This effect can be simulated by rotating the composite in Figure 9e 5° clockwise about the DWNT axis and then recalculating the simulation, as in Figure 9g. The microstructure in Figure 9b cannot however be produced from a similarly oriented fragment of 4H PbI$_2$ as the alternating nature of this structure would cause staggering of the iodine and lead columns rather than the superposition observed in the experimental and simulated fragment.

A minority product in the CCVD synthesis of DWNTs is small quantities of SWNTs, including a few examples of wide tubules. In Figure 10 we see an example of a ca. 4 nm diameter SWNT filled with PbI$_2$. The main reconstructed phase image in Figure 9a actually shows two nanotubes, the wide SWNT and also a narrower filled DWNT which consists of an inner tube of ca. 1.7 nm diameter and an outer tube of ca. 2.4 nm diameter. The microstructure of the PbI$_2$ in this second nanotube is tilted off axis and is not possible to discern. The PbI$_2$ crystal in the larger SWNT is highly crystalline, and the detail of the microstructure in Figure 10b shows that it consists of groups of atom columns arranged into diamonds. A power spectrum (**I** in Figure 10c) indicates that the crystal could possibly be either a 2H crystal
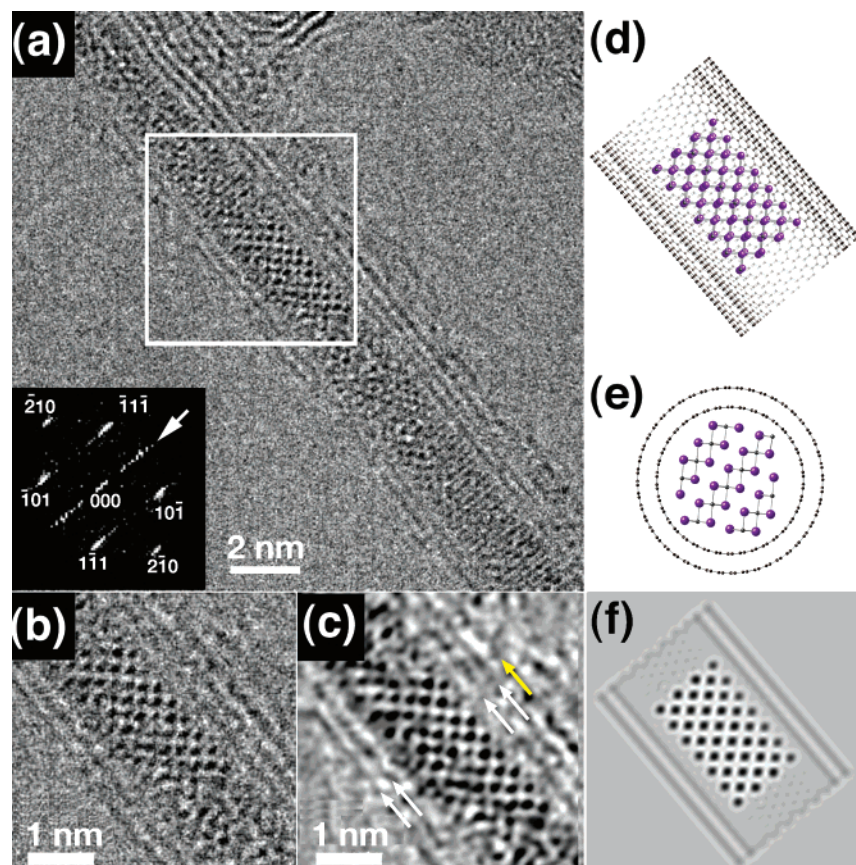
Figure 8. (a) Conventional HRTEM image of a 2.5 nm i.d. DWNT filled continuously with PbI$_2$. The inset power spectrum obtained from the indicated region in the main image is indexed according to a $\langle 121 \rangle$ projection. (b and c) Detail and noise-filtered image of the indicated region in a. (d and e) Side-on and end-on models of the derived model of the PbI$_2$/DWNT composites. (f) Scherzer defocus image produced from the model in d.
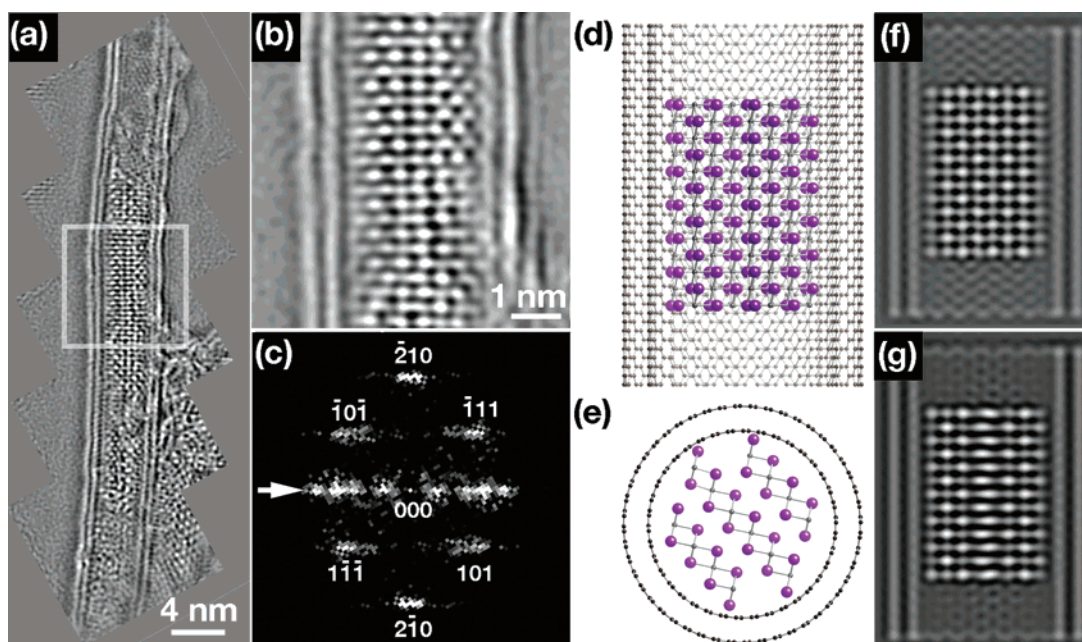

Figure 9. (a and b) Restored HRTEM phase image and detail of a 2.5 nm i.d. DWNT filled continuously with PbI$_2$. (c) Power spectrum obtained from the indicated region in a and indexed according to a $\langle \bar{1}21 \rangle$ projection. (d and e) Side-on and end-on models of the derived model of the PbI$_2$@DWNT composites. (f) Multislice simulation of the image phase produced from the model in d. (g) As for d but rotated 5° about the DWNT axis relative to the orientation depicted in e.

orientated along the $\langle 001 \rangle$ stacking direction or a 4H crystal oriented along its equivalent $\langle 001 \rangle$ stacking direction, as shown by the calculated and indexed electron diffraction patterns in Figure 10c **II** and **III**, respectively. The arrangement of atoms in these two projections is shown for 2H (top)

and 4H (bottom) in Figure 10d. Additionally, an end-on view of fragments of these two polytypes is given in Figure 10e (2H (top) and 4H (bottom)) from which we can see that the crystal fragment in both cases are viewed orthogonal to the stacking direction of the 2H and 4H forms. Image simulations
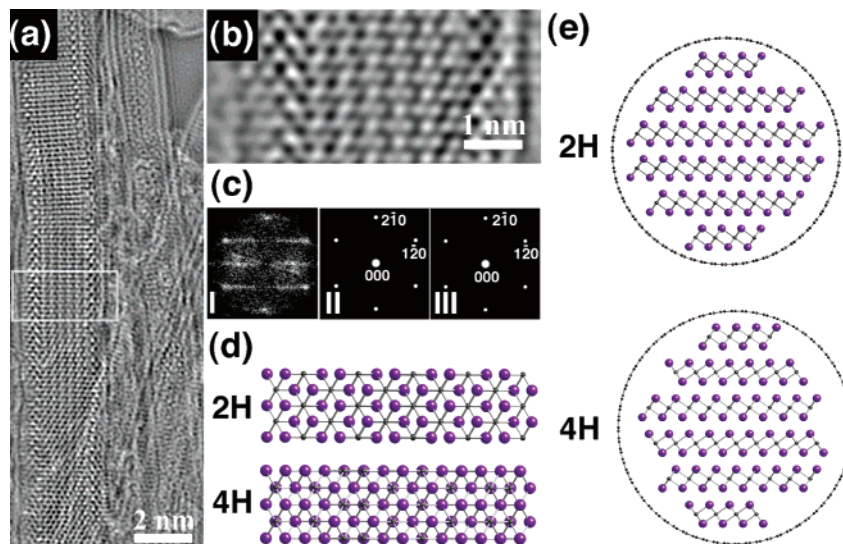
Figure 10. (a and b) Restored HRTEM phase image and detail of a 4 nm diameter SWNT filled continuously with PbI₂. (c) Experimental (**I**) and calculated power spectra of 2H (**II**) and 4H (**III**) fragments both projected along the equivalent ⟨001⟩ stacking direction. Note that in this projection the indexing is identical for both 2H and 4H. (e) End-on models showing the predicted relative stacking behavior of the 2H (top) and 4H (bottom) fragments in d modeled inside a ca. 3.7 nm SWNT.

(not shown) could not provide a quantitative distinction in terms of interpreting the obtained image contrast in particular as it was not possible to determine the precise thickness of the crystal fragment in Figure 10b. We therefore cannot unambiguously assign this fragment to either the 2H or the 4H form of PbI₂.

(iii) Washing Out Behavior of PbI₂. Filled carbon nanotubes CNTs have been envisaged as potential drug-delivery media.[32] This implies that it must be possible to fill them with biologically active materials (e.g., radionuclides)[33] and then release the filling. The first attempts to empty KI- or ZrCl₄-filled arc-synthesized SWNTs[24] were unsuccessful, and only the extraneous material could readily be removed, even after long-term washings in boiling aqueous media. Subsequently, it has been possible to wash out radioactive NaI or AgNO₃ introduced into SWNTs from solution[33] and MOH (M = Na and Cs) introduced into SWNTs from the melt.[34] We were able to release PbI₂ from most of the CCVD-synthesized DWNTs by refluxing them in 10 M NaOH for 12 h at 90 °C. This was confirmed by both TEM observation and EDX analysis (Figure 11), performed on both as-filled DWNTs and the NaOH-washed sample. Similar experiments attempted with arc-synthesized SWNTs revealed that the washing out of PbI₂ was less successful, and we think that this is largely due to the relative differences in diameter populations between the filled SWNT samples and the filled DWNT samples. Theoretical studies indicate that the length of the CNTs should not have an important influence on the emptying of the CNTs,[35] although the influence of the tubule diameter was taken into account.
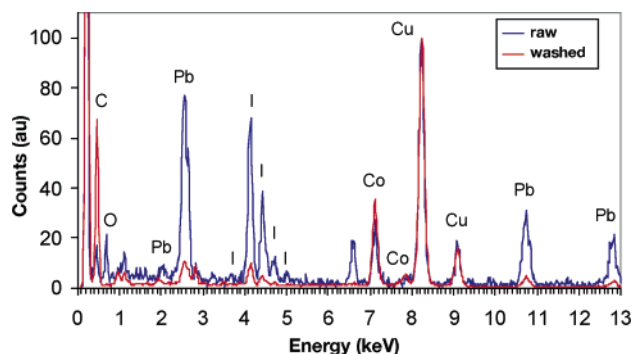

Figure 11. Normalized EDX spectra obtained from approximately similarly sized bundles of CVD DWNTs before (blue) and after (red) washing with dilute NaOH.

A further important factor may also be the aspect ratio of the included material. In general, nanotubes filled from solution contain small clusters of filling whereas melt-filled nanotubes are continuously filled. This will affect the diffusion path of the solvent molecules along the nanotubes. An additional factor concerns the tightness of fit of the crystals inside the nanotubes and the relative rigidity of the latter. Crystals introduced into wider multiwalled nanotubes from solution tend to be facetted, whereas melt-filled tubes tend to be filled more completely along their cross-section. In addition, we conclusively demonstrated that SWNTs readily distort in a complimentary fashion to a filling material which has an asymmetric cross section, as in the case of CoI₂.[7]

(iv) Raman Spectroscopy of PbI₂-Filled Nanotubes. The Raman spectra of 2H, 4H, and 12R polytypes of PbI₂ were described in detail by Sears et al.[36] All three polytypes exhibit the main three modes at 74 cm⁻¹ (E_g), 95 cm⁻¹ (A_{1g}), and 111 cm⁻¹, although there is no unambiguous symmetry assignment.[37] Figure 12a shows the Raman spectra of unfilled

(32) Salvador-Morales, C.; Flahaut, E.; Sim, E.; Sloan, J.; Green, M. L. H.; Sim, R. B. *Mol. Immunol.* **2006**, *43*, 193.

(33) Wu, S. W.; Guo, J. X.; Li, Y. L.; Huang, X.; Li, W. X. *Nanotechnology* **2003**, *14*, 1203.

(34) Thamavaranukup, N.; Höppe, H. A.; Ruiz-Gonzalez, L.; Costa, P.; Sloan, J.; Kirkland, A. I.; Green, M. L. H. *Chem. Commun.* **2004**, 1686.

(35) Waghe, A.; Rasaiah, J. C.; Hummer, G. *J. Chem. Phys.* **2002**, *117*, 10789.

(36) Sears, W. M.; Klein, M. L.; Morrison, J. A. *Phys. Rev. B* **1979**, *19*, 2305.

(37) Winkler, B.; Dove, M. T.; Salje, E. K.; Leslie, M.; Palosz, B. *J. Phys.: Condens. Matter* **1991**, *3*, 539.
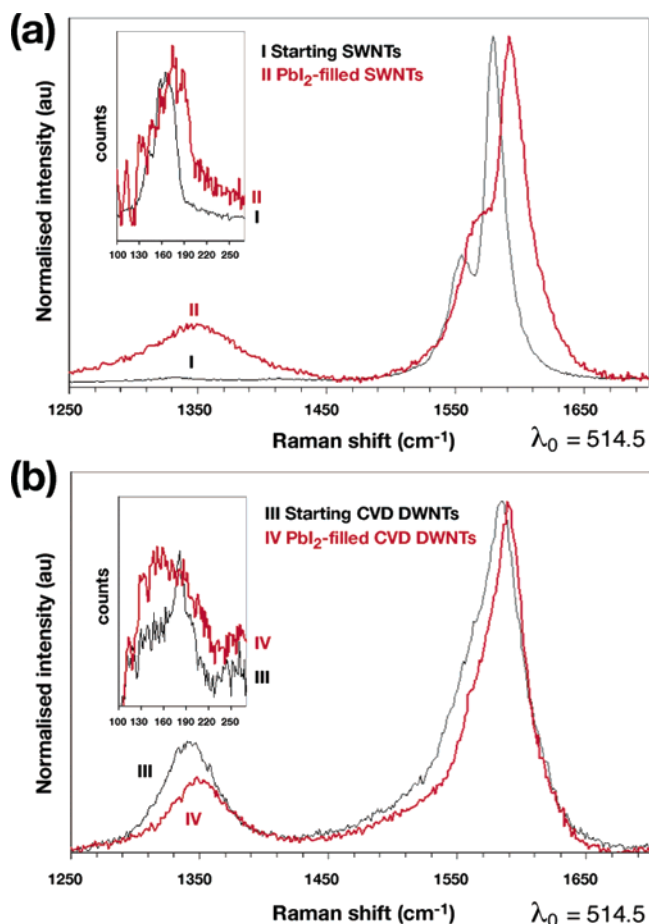
Figure 12. (a) Raman spectra obtained from unfilled (**I**) and filled (**II**) SWNTs. The RBM region at low wavenumbers is shown in the inset. (a) Raman spectra obtained from unfilled (**III**) and filled (**IV**) DWNTs. The RBM region at low wavenumbers is shown in the inset.

SWNTs (i.e., **I** in Figure 12a) and PbI$_2$-filled SWNTs (i.e., **II** in Figure 12a). The spectra are noisy due to a limited acquisition time in order to avoid heating of the samples. Figure 11b shows spectra recorded for unfilled CVD DWNTs (i.e., **I** in Figure 12b) and PbI$_2$-filled CVD DWNTs (i.e., **II** in Figure 12b). A shift of the G band toward higher wavenumbers was observed in both cases (i.e., from 1579 to 1591 cm^{-1} for the SWNTs and from 1586 to 1589 cm^{-1} for the DWNTs). The two components of the G band for the SWNTs (1555 and 1579 cm^{-1}) were merged into a shoulder at 1563 cm^{-1} after filling. No significant modification of the radial breathing modes (RBM) signals (low-frequency range) was observed, although there was possibly a small upshift of the peaks again for the SWNT sample. The ratio between the intensity of the D and G bands (denoted $I_{D/G}$ hereafter) increased significantly (from 3% to 18%) due to filling in the case of the PbI$_2$-filled SWNTs. On the contrary, $I_{D/G}$ decreased from 30% to 20% in the case of the PbI$_2$-filled DWNTs. The increase in the $I_{D/G}$ ratio due to filling has already been reported[38] and could be interpreted as an increase in the disorder within the samples due to the filling process, although the clear interpretation of the D band is still in debate. Similar results were observed in the case of the DWNT sample, as shown in Figure 12b. A small

upshift of the G band was also observed (from 1584 to 1588 cm^{-1}). A small upshift of the RBM peaks was also observed, although it was often difficult to reproduce the same pattern in different places of the same sample. Systematic analysis of data from another Raman study (spectra obtained with 785 nm excitation wavelength of both pristine and filled nanotubes at various laser power densities)[39] however revealed no noticeable change in the position or the number of the main components of the RBM bands of the pristine and PbI$_2$@DWNTs, which would be an indication of an undetectable amount of charge transfer occurring between the carbon nanotubes and PbI$_2$.

In the case of CNTs doped with C$_{60}$ molecules (i.e., so-called peapods), no shift of the G band was observed although a downshift occurred in the RBM range.[40,41] This downshift was explained by electron charge transfer from C$_{60}$ to the CNTs. Doping CNTs with electron acceptors (oxidizing compounds) such as CrO$_3$ has already been reported to induce an upshift of the tangential modes.[42] Cambedouzou et al. also reported an upshift of the tangential mode as a possible consequence of charge transfer between iodine and the CNTs in the case of I$_2$-doped DWNTs.[43] No Raman signal corresponding to 2H, 4H, or 12R PbI$_2$ could be observed in the washed DWNT samples, confirming once more that this material was successfully removed from these samples by the gentle NaOH washing.

Discussion

Our results confirm that PbI$_2$ may be introduced from the melt into both SWNTs and DWNTs of widely differing diameters. Under the conditions of formation, we might expect that the filling material might contain a significant quantity of 4H PbI$_2$ as the programmed heating of the introduced material confirmed that 2H PbI$_2$ readily converts to 4H PbI$_2$ under the conditions of filling. Only in one instance have we been able to observe 4H-type PbI$_2$ formed within SWNTs of at least 2 nm in diameter, and we have not been able to unambiguously confirm its presence in DWNTs. In very narrow DWNTs PbI$_2$ does not crystallize and a noncrystallizing filling is instead obtained, whereas in the case of SWNTs with similar diameters, crystallization is always observed.

Clearly both SWNTs and DWNTs place constraints on the mode of crystal growth of PbI$_2$, but the reasons for the clear selectivity of the 2H form versus the 4H form, especially in wider nanotubes, are as yet unclear. The rigidity of the encapsulating nanotube seems to play a role in whether the filling obtained is crystalline or noncrystalline, as in the case of narrow, rigid DWNTs versus SWNTs, but as the filling of these nanotubes occurs from the melt under relative

(38) Bendiab, N.; Anglaret, E.; Sauvajol, J. L.; Duclaux, L.; Béguin, F. *Chem. Phys. Lett.* **2001**, *339*, 305.

(39) Sendova, M.; Flahaut, E.; De Bono, B. Z. *J. Appl. Phys.* **2005**, *98*, 104304.

(40) Bandow, S.; Takizawa, M.; Hirahara, K.; Yudasaka, M.; Iijima, I. *Chem. Phys. Lett.* **2001**, *337*, 48.

(41) Bandow, S.; Takizawa, M.; Kato, H.; Okazaki, T.; Shinohara, H.; Iijima, I. *Chem. Phys. Lett.* **2001**, *347*, 23.

(42) Corio, P.; Santos, A. P.; Santos, P. S.; Temperini, M. L. A.; Brar, V. W.; Pimenta, M. A. Dresselhaus, M. S. *Chem. Phys. Lett.* **2004**, *383*, 475.

(43) Cambedouzou, J.; Sauvajol, J. L.; Rahmani, A.; Flahaut, E.; Peigney, A.; Laurent, C. *Phys. Rev. B* **2004**, *69*, 135422:1−6.

slow-cooling conditions, kinetic (i.e., rapid) filling conditions are not necessarily observed under the conditions of our experiments. Wilson's dynamic simulations of liquid KI introduced into different diameter SWNTs[8] indicate that the ordering of this material into 2×2, 3×3, etc., continuous crystals proceeds over a picosecond time scale, which indicates that it is probably not possible to directly image and observe crystal growth from the melt inside carbon nanotubes using any instrumentation currently available, assuming that this could be achieved in situ. However, we must assume that crystal growth within carbon nanotubes is largely a kinetic phenomenon and that control over crystal growth is not likely to be largely influenced by the small differences in energy between the various polytype forms of PbI$_2$. Control over crystal growth within nanotubes is more likely to be driven by space-filling considerations, and it may be that the more regular 2H form of PbI$_2$ packs more readily into nanotubes than the 4H form. It also seems likely that once the habit of the obtained crystal is fixed in place by the encapsulating tubule, then the relative orientation of successive PbI$_2$ octahedral layers formed in the wider diameter tubules is unlikely to change during the cooling phase of the experiment. The narrower nanotubes do not give the option of forming the 4H structural form as they are simply too narrow to permit formation of more than one PbI$_2$ layer in cross-section. In the case of SWNTs, these can distort in order to accommodate the asymmetric PbI$_2$ fragments that form as a result (see Figure 4h). In the case of the narrowest DWNTs, these are unable to distort and a noncrystallizing filling is obtained instead.

These crystallizing phenomena will have important consequences for the physical properties of nanotube-included PbI$_2$. Greater selectivity for the 2H form is clearly observed which will influence the efficiency of its usage as a detector material given that this is correlated with the number and type of polytypes present in a given sample. In the narrower confined crystals changes in the local Pb^{2+} coordination on the surfaces of the PbI$_2$ crystals may have an impact on these properties, although this has not yet been quantified.

Conclusions

The capillary method has been used successfully to grow 1D crystals of PbI$_2$ within single-walled and double-walled carbon nanotubes, and we have found that the diameter of the host SWNT profoundly influences the obtained structure of the filling material. The reduction of the coordination of the ions in the periphery of the nanotubes, due to the confinement into the capillaries, has been demonstrated. Both SWNTs and DWNTs have a strong preference for growing 2H-type PbI$_2$ as opposed to the 4H form, even though the latter was demonstrated to form readily under the experimental conditions. Only one isolated instance of 4H formation was observed in a comparatively wide SWNT. In rigid, narrow DWNTS, PbI$_2$ does not crystallize and instead forms an amorphous filling, an effect attributed to the comparative rigidity of these narrow tubules. Characterization of the electrical properties of individual PbI$_2$-filled DWNTs is in progress and should bring new data about the possible interactions between PbI$_2$ and the carbon nanotubes.